Published in *Materials Science and Engineering A*, 2015, 638, pp174-182. doi: 10.1016/j.msea.2015.04.053

A critical examination of pure tantalum processed by high-pressure torsion

Nicolas Maury[a], Nian Xian Zhang[b], Yi Huang[b], Alexander P. Zhilyaev[c,d], Terence G. Langdon[b,e,*]

[a]École Nationale Supérieure des Ingénieurs en Arts Chimiques et Technologiques (ENSIACET), National Polytechnic Institute of Toulouse (INPT), 31077 Toulouse CEDEX 04, France
[b]Materials Research Group, Faculty of Engineering and the Environment, University of Southampton, Southampton SO17 1BJ, U.K.
[c]Institute for Metals Superplasticity Problems, Russian Academy of Sciences, 39 Khalturina, 450001 Ufa, Russia
[d]Research Laboratory for Mechanics of New Nanomaterials, St. Petersburg State Polytechnical University, St. Petersburg 195251, Russia
[e]Departments of Aerospace & Mechanical Engineering and Materials Science, University of Southern California, Los Angeles, CA 90089-1453, U.S.A.

[*] Corresponding author: Terence G. Langdon; e-mail: langdon@usc.edu

Abstract

Tantalum, a common refractory metal with body-centred cubic (BCC) crystalline structure, was processed by high-pressure torsion (HPT) at room temperature through different numbers of rotations. Significant grain refinement and high strength were achieved with a reduction in grain size from ~60 μm to ~160 nm and an increase in strength from ~200 to >1300 MPa. Hardness measurements revealed a high level of homogeneity after 10 turns of HPT but the hardness after 10 turns was slightly lower than after 5 turns indicating the occurrence of some recovery. Tensile testing at a strain rate of 1.0×10^{-3} s^{-1} gave high strengths of ~1200 MPa but little or no ductility after processing through 1, 5 and 10 turns. The introduction of a short-term (15 min) anneal immediately after HPT processing led to significant ductility in all samples and a reasonable level of strength at ~800 MPa.

Keywords: Electron backscatter diffraction; hardness; high-pressure torsion; tantalum, ultrafine grains

Introduction

Tantalum is a refractory body-centred cubic (BCC) metal having very good room temperature ductility (>20% tensile elongation) [1]. It is generally considered an excellent material for use in shaped charges and explosively forged projectiles due to its high density (16.7 g cm^{-3}), superior strength and good ductility over a very wide range of strain rates and temperatures [2]. Because it is chemically inert, tantalum is used widely in the chemical industry particularly as valves, heat exchangers and bayonet heaters [1,3]. Since it is also highly bioinert, it is used for orthopedic implants [4] and the elasticity of tantalum makes it especially appropriate for use in hip replacements to avoid stress shielding [5]. Generally, there is significant interest in making use of tantalum instead of titanium for medical prostheses but, in order to make Ta comparable to Ti as a potential implant material, it is necessary to improve the material strength.

The grain size of a material is the major microstructural parameter dictating the properties of a polycrystalline solid at room temperature. However, the application of traditional plastic working techniques to tantalum, such as rolling and extrusion, generate relatively coarse-grained microstructures [6,7]. With reference to the Hall-Petch relationship [8,9], it is reasonable to anticipate that the strength and performance of tantalum will be significantly improved if it is possible to produce an ultrafine-grained (UFG) or a nanostructured material.

It is now well-established that significant grain refinement may be introduced in bulk polycrystalline materials through the application of severe plastic deformation (SPD) [10-12] since the grain sizes produced by SPD processing are typically within the submicrometer or even the nanometer range. Various SPD techniques are now available but most attention has been centred on the two procedures of equal-channel angular pressing (ECAP) [13] and high-pressure torsion (HPT) [14]. Extensive experiments have shown that processing by HPT is especially attractive because, by comparison with ECAP, it produces smaller grains [15,16]

and a higher fraction of grain boundaries having high angles of misorientation [17]. In practice, processing by ECAP and HPT has been successfully applied to a wide range of metals having face-centred cubic (FCC) and hexagonal close-packed (HCP) crystal structures but there are relatively few investigations of the SPD processing of BCC metals. Specifically, for tantalum there are several reports of processing and microstructural refinement using either ECAP [18-21] or HPT [22-26] but the experimental results from the HPT processing are very limited because they concentrate primarily on dynamic testing at strain rates in the range of ~10^3 s^{-1} using a split Hopkinson bar [22], the compression of micro-pillars in a scanning electron microscope [25] and the application of shock compression generated by high-energy laser pulsing [26]. There are two reports documenting hardness measurements in samples of Ta processed by HPT but these investigations were designed specifically to compare the hardness values obtained from a very wide range of FCC, HCP and BCC metals [23,24].

It follows from this summary that there has been no systematic study of the evolution of microstructure and the mechanical properties of tantalum when using HPT processing. Accordingly, the present research was initiated to address this deficiency by providing a detailed evaluation of microstructural evolution in tantalum during HPT processing, measuring the mechanical properties in tensile testing at room temperature using a strain rate of 1.0×10^{-3} s^{-1} and examining the effect on the tensile properties of short term (15 min) annealing in the post-HPT condition. Based on these results, the overall objective was to establish a procedure that may be used to enhance the properties of this material for use in bio-applications. An earlier report described some of the preliminary results obtained in this research [27].

Experimental material and procedures

The experiments were conducted using tantalum of 99.9% purity which was received in an annealed condition as a rod with a diameter of 10 mm. The rod was sliced into discs with thicknesses of ~1.2 mm and these discs were then ground with abrasive papers to final thicknesses of ~0.8 mm for HPT processing. The processing was conducted at room temperature under quasi-constrained conditions [28, 29] through total numbers of turns, *N*, of 0.5, 1, 2, 5 and 10 using an imposed pressure of 6.0 GPa and a rotational speed for the lower anvil of 1 rpm.

Following HPT processing, discs in both the as-received condition and those processed by HPT were hot mounted in bakelite, ground with abrasive papers, and then a final polish was performed using a colloidal silica solution in order to produce a mirror-like surface. For the as-received sample, the polished surface was etched using the ASTM 163 etchant which consists of 30 mL of water, 30 mL of sulphuric acid (H_2SO_4), 30 mL of hydrofluoric acid (HF) and 3 to 5 drops of 30% hydroxide peroxide (H_2O_2) with an etching time of 20 to 40 s. The sample surface was then observed in dark field using an Olympus BX51 optical microscope in order to determine the initial grain structure. The grain size was measured by the linear intercept method using Image J software. The grain structure after HPT processing was examined by electron backscattered diffraction (EBSD) using a JSM6500F thermal field emission scanning electron microscope (SEM). The EBSD patterns were collected using a step size of 50 nm and a cleaning procedure was applied such that the total number of modified points was less than 10% of the total points measured. High-angle grain boundaries (HAGBs) were defined by the software as boundaries having misorientation differences between adjacent measuring points of more than 15° and low-angle grain boundaries (LAGBs) were defined as having misorientation differences of 2° – 15°. More than 300 grains were measured for estimating the average grain size.

The values of the Vickers microhardness, Hv, were measured on the polished surfaces and the distributions of the hardness values are presented by mapping the values of Hv over the total surface of each disc. In practice, the individual values of Hv were recorded following a rectilinear grid pattern with a separation of 0.3 mm between each consecutive point as described in an earlier report [30]. The hardness measurements were taken using an FM300 hardness tester equipped with a Vickers indenter with a load of 300 gf and a dwell time of 15 s. All of the individual values of Hv were used to construct colour-coded contour maps that provided a clear visual presentation of the distributions in hardness across the surface of each disc.

The X-ray diffraction (XRD) analyses were conducted over the HPT disc surfaces and the samples processed by HPT were evaluated using a Bruker D2 Phaser X-ray diffractometer equipped with a Cu target using Cu Kα (λ = 0.15406 nm) radiation. The X-ray samples were prepared from the HPT-processed discs by conventional metallographic grinding and polishing and then the discs were slightly etched for 5-10 s using the ASTM 163 etchant to remove the thin deformed surface layer. Scans were performed of θ - 2θ from 2θ = 30° to 100° to record the XRD patterns and the crystal sizes and microstrains were calculated based on the Rietveld method [31] using Maud software to accomplish the profile fitting. The texture option was applied when using the Maud software and the crystal size and microstrain were used to estimate the values of the dislocation density.

To evaluate the effect of short-term annealing in the post-HPT condition, some samples were annealed for a short time of 15 min at either 873 or 973 K immediately after the HPT processing. These annealing temperatures were selected based on earlier reports presenting the Vickers hardness measurements as a function of annealing temperature for extruded tantalum and showing that the hardness begins to drop from 973 K and reaches a softening plateau at ~1173 – 1223 K [18,19]. To avoid recrystallization which may cause

strength loss and grain growth in HPT-processed samples, a very short annealing time was used at temperatures of 873 or 973 K.

Tensile specimens were cut from the as-received sample, the HPT-processed samples and the samples subjected to post-HPT annealing. Following earlier practice [32], and in order to avoid any microstructural inhomogeneities in the centres of the discs, two tensile specimens were prepared from each disc using electro-discharge machining with these specimens arranged symmetrically on either side of the disc centre. The miniature tensile specimens had gauge lengths and widths of 1 mm. These specimens were then tested in tension at room temperature using a Zwick 30 KN Proline testing machine operating at a constant rate of cross-head displacement with an initial strain rate of 1.0×10^{-3} s^{-1}.

Experimental results

Microstructure before and after HPT processing

In the initial as-received condition, the material had a uniform equiaxed microstructure with an average grain size of ~60 μm and an average hardness of ~87 Hv.

The microstructures development during HPT processing are displayed in Fig. 1 where the centre and edge areas are shown after 0.5 and 10 turns in the top and bottom rows and the central row shows the edge areas after 1 and 5 turns, respectively: the colours denote different grain misorientations as depicted in the unit triangle on the right, low-angle boundaries (2°-15°) are shown in yellow and high-angle boundaries (>15°) are in black. It is apparent from the upper row that the edge experiences very significant grain refinement after 0.5 turn with a measured grain size of ~0.2 μm in Fig. 1(b) whereas in the centre area in Fig. 1(a) the structure remains coarse and similar to the as-received condition. As processing increases to 1 and 5 turns in Figs 1(c) and (d), there is some minor additional grain refinement at the edges of the discs with average grain sizes of ~160 and ~140 nm, respectively. After 10 turns in Fig. 1(f) and (e), the microstructure is essentially uniform

from the edge to the centre and the measured average grain sizes are similar at ~160 nm. Nevertheless, there is some evidence in Fig. 1(f) for the appearance of a very small number of slightly larger grains in the edge region of the disc after 10 turns and this indicates the onset of structural recovery. By contrast, there is no evidence for any structural recovery in the central region of the disc.

The grain size distributions after HPT processing are shown in Fig. 2 where (a) to (d) show the distributions near the edge of each disc after 0.5, 1, 5 and 10 turns and (e) shows the size distribution in the central region of the disc after 10 turns. For the edge regions, all distributions look reasonably similar but the average grain size is gradually reduced from ~200 nm after 0.5 turn to ~160 nm after 1 turn, ~140 nm after 5 turns and then ~160 nm after 10 turns. It is concluded from these measurements that a saturation level of ~160 nm is rapidly attained in the edge region of the disc even after only 1 turn. It is also apparent from Fig. 2(d) and (e) that the disc edge and centre areas have almost identical grain size distributions after 10 turns which confirms the development of a uniform microstructure in Ta processed by HPT.

Details on the grain misorientation distributions are given in Fig. 3 where (a) and (b) show the edge and centre after 0.5 turn, (c) and (d) show the edge regions after 1 and 5 turns and (e) and (f) show the edge and centre after 10 turns, respectively: each plot records the percentage of high-angle grain boundaries where high-angle boundaries are defined as misorientations >15°. It should be noted that the misorientation distributions shown in Fig. 3 correspond to the conventional pixel-to-pixel distributions recorded by orientation imaging and this may not correspond precisely to the grain-to-grain misorientation distributions [33]. After 0.5 turn as shown in Figs 3 (a) and (b), there is a very significant difference across the disc with a high fraction of ~53% of high-angle grain boundaries in the edge region but only ~22% in the central region. Higher fractions of high-angle boundaries are recorded at the

edges after 1, 5 and 10 turns as shown in Figs 3(c), (d) and (e) and after 10 turns the fractions are ~61% at the edge in Fig. 3(e) and ~59% in the centre in Fig. 3(f).

Hardness evolution during HPT processing

In order to obtain a comprehensive impression of the hardness distributions throughout the surfaces of the discs after HPT processing, the hardness values for all discs are displayed pictorially as colour-coded contour maps in Fig. 4 where the upper row is for 0.5, 1 and 2 turns, the lower row is for 5 and 10 turns and the individual values of Hv are represented by a set of unique colours denoting values from 50 to 550 in incremental steps of 50 as shown by the colour key on the right: in these plots, the coordinate system *X* and *Y* denotes two randomly selected perpendicular axes that are superimposed on the discs such that the central point in every disc is given by the coordinates (0, 0)

The results in Fig. 4 show a large central region of lower hardness after 0.5 turn but this region is gradually removed with further straining so that ultimately, after 10 turns, the central area of lower hardness is exceptionally small. It is important to note also that these colour-coded maps are symmetrical around the central points and this demonstrates that the hardness values recorded from linear traverses along randomly selected diameters, as presented earlier [27], provide a valid representation of the overall behaviour over the disc surface. Furthermore, even though a good level of hardness homogeneity is attained after 10 turns, the results show also that the overall hardness values after 10 turns are slightly lower than the hardness values in the edge areas after 5 turns. Thus, by comparison with the disc for 5 turns, this variation leads to a slightly different colour for the overall appearance of the disc after processing by HPT through 10 turns.

Microstructural results from the X-ray line profile analysis

The XRD patterns of the as-received Ta and samples processed by HPT are shown in Fig. 5 for different numbers of turns. The diffraction peaks are marked with the relevant

reflection planes and it is apparent that, as the numbers of rotations increase, the (202) and (013) peaks gradually disappear whereas the intensities of the (110), (200) and (112) peaks decreases. The XRD shows no evidence for a phase transformation during the processing of tantalum by HPT. In addition, the peaks of the HPT samples show line broadening by comparison with the as-received material and this broadening may be used to estimate the crystallite sizes for each processing condition [34,35].

Figure 6 shows the crystallite sizes and microstrain based on analysis of the X-ray diffraction line broadening with the error bars taken from the Maud calculations. These measurements demonstrate that the crystallite sizes after 1, 5 and 10 turns are measured as ~69, ~58 and ~65 nm, respectively, and these values are significantly smaller than the grain sizes recorded by EBSD near the edges of the discs where, as shown in Fig. 2, the corresponding grain sizes were ~160, ~140 and ~160 nm, respectively. It is now well established that the crystallite sizes determined by XRD are consistently smaller than the grain sizes measured by EBSD or TEM [36] and this is because XRD measures the mean size of the domains which scatter X-rays coherently whereas EBSD or TEM provides a measure of the sizes of grains separated by boundaries having higher angles of misorientation [37].

The microstrain measured from the XRD peak broadening is shown in Fig. 6 and this mainly represents the concentration of crystalline defects in the processed samples. It is evident that the microstrain increases with increasing numbers of HPT rotations from 1 to 5 turns but thereafter it decreases from 5 to 10 turns. A decrease in microstrain from 5 to 10 turns matches the hardness values where the measured hardness in the saturation region at the edge of the disc after 10 turns is slightly lower than the hardness measured after 5 turns.

From the microstructure and hardness results in Figs 1 and 4, it is apparent that the microstructures are inhomogeneous at lower numbers of turns and as the numbers increase both the hardness and the microstructures tend to become more homogeneous. Since the

XRD analysis was performed over the HPT disk surfaces, this includes a wide range of evolutionary levels of microstructure especially when N is small. Thus, the XRD results at low numbers of turns include the microstructure contributions from fine grains in the disc edge area to the coarser grains in the disc centre area, whereas the XRD results at high numbers of turns include the microstructure contributions from fine grains at the disc edge through to fine grains in the disc centre area.

The effect of post-deformation annealing on the tensile properties

The results from the tensile testing are shown in Fig. 7 for the as-received sample and after (a) 1, (b) 5 and (c) 10 turns. For each processing condition, the as-received material (lower curve) shows low strength of ~200 MPa but with relatively good ductility whereas the HPT processed sample (upper curve) shows high strength up to >1000 MPa but little or no ductility. It is now well established that the mechanical properties of samples processed by ECAP may be significantly improved, and especially the ductility may be increased, by subjecting the samples to short term annealing after processing [38-40] and a similar effect was demonstrated recently for samples processed by HPT [41]. Accordingly, the processed samples were subjected to short-term anneals of 15 min at either 873 or 973 K and the results are shown as the two intermediate curves in Figs 7(a)-(c).

Inspection of Fig. 7 leads to broad conclusions concerning the effect of a short-term anneal after HPT processing on the tensile properties at an initial strain rate of 1.0×10^{-3} s^{-1}. First, after 1 turn of HPT the strength is >1300 MPa but there is only limited ductility whereas an anneal at 873 K reduces the strength to >1000 MPa and there is a reasonable level of ductility. The result for N = 1 turn contrasts with the data for 5 and 10 turns where the anneal at 873 K retains the strength at >1000 MPa but the materials are inherently brittle. By contrast, a short-term anneal of only 15 min at 973 K has a major effect because for each processing condition of 1, 5 and 10 turns the strength is retained at ~800 MPa and all

specimens exhibit good ductility with overall elongations to failure of ~35%. These results demonstrate that a post-HPT short-term anneal of 15 min at 973 K is beneficial for tantalum because the material retains much of the high strength introduced by HPT while at the same time exhibiting a reasonable level of ductility.

Discussion

Microstructural characteristics after HPT

It is well established that the strain imposed in HPT varies significantly across the disc and in practice the equivalent von Mises strain, ε, may be estimated from the relationship [42-44]

$$\varepsilon = \frac{2\pi N r}{h\sqrt{3}} \qquad (1)$$

where N is the number of turns imposed in HPT and r and h are the radius and height (or thickness) of the disc, respectively. It follows from eq. (1) that the strain is zero at the centre of the disc where $r = 0$ and it reaches a maximum value at the outer edge. These calculations readily account for the significant differences in the grain size and boundary misorientation distributions between the edge and central regions as shown in Figs 2 and 3.

The results obtained in this investigation show that processing by HPT produces very significant grain refinement in tantalum of 99.9% purity. Specifically, the as-received grain size of ~60 μm is refined to ~160 nm at the edge of the disc after only 1 turn. Furthermore, there is excellent homogeneity when the processing is continued to 10 turns so that the grain size is ~160 nm throughout the disc and the fractions of high-angle grain boundaries are ~61% at the edge and ~59% in the centre. The development of microstructural uniformity during processing by HPT, as demonstrated in the present results for tantalum, is consistent with a theoretical approach based on the application of strain gradient plasticity modelling [45].

The average grain size attained after HPT processing compares very favourably with the grain sizes reported earlier after processing tantalum by ECAP at room temperature. For example, there are reports of grain sizes of ~285 nm after 4 passes of ECAP using a 90° ECAP die and processing route C where the billet is rotated by 180° between each pass [19] and ~255 nm when using a similar ECAP facility and processing route B_C where the billet is rotated in the same sense by 90° between each pass [18]. As anticipated from earlier results [15,16], processing by HPT and ECAP at the same temperature leads to smaller grains when using HPT.

In practice, it is apparent from Fig. 1(e) that some relatively coarser grains appear in the edge area of the disc after processing by HPT through 10 turns. A similar result was also reported in the HPT processing of niobium [46] where it was assumed that the microstructure recovers at the expense of grain boundary migration [47]. There is also a possibility of texture-induced grain coalescence in which several grains of similar orientations come together so that the boundaries between them develop as new low-angle boundaries and the subsequent merging of the grains leads to the generation of a new coarser structure. This was observed recently in a low-carbon steel processed by ECAP where grain coarsening was attributed to the evolution of a crystallographic texture [48]. In practice, coarsening can take place by the coalescence of adjacent grains if their disorientations become sufficiently low and a decrease in disorientation may be explained by the plastic strain which arises from the convergence of the orientations of adjacent grains that are initially separated by larger angles. Thus, as they approach the same ideal orientation, the orientation difference decreases and they are able to coalesce into a single grain.

In FCC metals, slip generally occurs on {111} planes in <110> directions and the perfect Burgers vector is $a/2$ <110> where a is the lattice parameter and this is a close-packed direction representing the shortest repeat length in the crystal. The {111} slip planes have the

largest interplanar spacing of those containing close-packed directions. However, slip is more complex in BCC crystals. Generally, slip occurs in the closest packed <111> direction and the Burgers vector is *a*/2 <111>. The planes with the largest interplanar spacing are {110} followed by {112} and then {123}. An examination of Fig. 1 shows there are many grains that are reasonably green in colour corresponding to grains having their {110} plane parallel to the disc surface and there are also some grains that are pink in colour corresponding to grains having their {112} planes parallel to the disc surface. In Figs 1 (a), (c), (d) and (e), representing the edge regions of the discs, the fractions of blue grains are reduced with increasing numbers of turns. In practice, the torsion strain is applied in a direction parallel to the disc surface so that slip occurs on the {110} and {112} planes to accommodate the severe torsional strain. Furthermore, since tantalum has a relatively high stacking fault energy [49], this facilitates the movement of dislocations within its crystal structure.

For materials subjected to SPD processing, the dislocation density, ρ, may be calculated using the relationship [50-52]:

$$\rho = \frac{2\sqrt{3}\left\langle \varepsilon^2 \right\rangle^{\frac{1}{2}}}{D_c \times b} \qquad (2)$$

where ε and D_c are the microstrain and the crystallite size in XRD, respectively, and b is the Burgers vector which is equal to $\sqrt{3}a/2$ for BCC metals. The calculated values for the dislocation density are shown in Fig. 8 as a function of the numbers of turns and, by comparison with Fig. 6, it is readily apparent that the dislocation density and the microstrain exhibit similar behaviour. In practice, the dislocation density increases initially from ~1.8 × 10^{14} m^{-2} after 1 turn to ~2.3 × 10^{14} m^{-2} after 5 turns and then decreases again to ~1.4 × 10^{14} m^{-2} after 10 turns. The decrease in the dislocation density between 5 and 10 turns confirms the occurrence of some recovery.

Hardness and tensile properties after HPT

It is apparent from inspection of Fig. 4 that initially, after 0.5 turn, the hardness is low in the disc centre area but high at the edge of the disc. This is consistent with the prediction of eq. (1). But as the numbers of turns increases to 1 and more, the hardness displays a two-phase behaviour which includes a lower hardness around the centre of the disc and a saturation plateau near the outer edges. The proportion of hardness values lying in the lower hardness region decreases with the numbers of turns and conversely the saturation plateau extends inwards to a greater extent with increasing numbers of rotations. The hardness reaches a reasonable level of homogeneity after 10 turns except for slightly lower values of Hv over a region of ±0.5 mm around the disc centre. The hardness at the edge of the disc after 10 turns is slightly lower than after 5 turns and this is consistent with the minor increase in grain size from ~140 to ~160 nm and with the presence of some slightly larger grains at the edge of the disc after 10 turns as shown in Fig. 1(e). The final hardness of Hv ≈ 400 after 10 turns is significantly higher than the maximum of Hv ≈ 234 ± 5 for tantalum processed by ECAP through 4 passes using route C [19].

It was shown in an early report that all of the hardness datum points derived in HPT processing may be conveniently correlated at every point by plotting the individual hardness values against the equivalent strain derived from eq. (1) [53]. This plot is shown in Fig. 9 where the values of the Vickers microhardness are plotted as a function of the equivalent strain. Inspection of Fig. 9 shows that after 1 turn the disc hardness tends to reach a saturation level near the edge and after 2, 5 and 10 turns the centre of each disc has not fully achieved a saturation level. The saturation hardness in Ta is Hv ≈ 430 and this is achieved at equivalent strains at and above ~20. The plot in Fig. 9 is typical of many metals and it corresponds to HPT processing in the absence of any significant recovery [54-56].

The difficulty of achieving both high strength and good ductility in materials subjected to SPD processing forms the so-called paradox of strength and ductility which specifically delineates the difficulty of attaining reasonable ductility in UFG metals [57]. It was shown very recently that both good strength and good ductility may be achieved in HPT processing by continuing the processing through sufficiently large numbers of turns [58,59] and the present results now demonstrate an alternative procedure of performing post-HPT short-term annealing. The results from the tensile testing shown in Fig. 7 are consistent with the conventional paradox of strength and ductility [57]. However, they demonstrate also the potential for achieving a significant increase in ductility with only a relatively small loss in strength through the simple procedure of performing a short-term (15 min) anneal immediately following the HPT processing. These results are therefore consistent with an earlier investigation where good ductility was also achieved in an FCC Al-1% Mg solid solution alloy by performing a short-term anneal after HPT processing [41]. In addition, the yield stresses of ~800 MPa in Fig. 8, which were achieved consistently in all specimens after short-term anneals at 973 K, are larger than the highest yield stress of ~670 MPa reported for tantalum after processing by ECAP [19]. Accordingly, it is concluded that excellent properties may be attained in tantalum, thereby contributing to the potential use of this material in bio-applications, by processing through a combination of HPT and short-term annealing of 15 min in the immediate post-HPT condition.

Summary and conclusions

1. Pure tantalum was successfully processed by high-pressure torsion at room temperature producing a reduction in grain size from ~60 μm to ~160 nm. The microstructure was markedly inhomogeneous after 0.5 turn but gradually developed into a reasonably homogeneous structure after 10 turns where the fractions of high-angle grain boundaries were ~61% and ~59% at the edge and centre of the disc, respectively.

2. The initial hardness in the annealed condition was ~87 Hv but the hardness increased to ~400 Hv after 10 turns. There is evidence from the hardness and grain size measurements for a small amount of recovery between 5 and 10 turns. From analysis of the X-ray diffraction data, it is shown that the microstrain and the dislocation density both exhibit similar variations with the numbers of HPT turns.

3. Tensile testing was conducted at an initial strain rate of 1.0×10^{-3} s^{-1} and the results show the initial annealed material exhibits a strength of ~200 MPa and good ductility but the strength is increased to ~1200 MPa with little or no ductility after HPT processing through 1, 5 and 10 turns.

4. The introduction of a short-term (15 min) anneal at 973 K immediately following HPT processing is effective in providing good ductility with overall elongations of ~35% while retaining a high level of strength at ~800 MPa. Thus, short-term annealing is effective in optimising the mechanical properties of pure tantalum after SPD processing.

Acknowledgements

This work was supported in part by the Russian Science Foundation under Grant No. 14-29-00199 (APZ) and by the European Research Council under ERC Grant Agreement No. 267464-SPDMETALS.

References

[1] R.W. Buckman, JOM 52 (3) (2014) 40-41.

[2] S. Nemat-Nasser, J.B. Isaacs, M. Liu, Acta Mater. 46 (1998) 1307-1325.

[3] C.W. Blake, Industrial and Energy Chemistry 27 (1935) 1166-1169.

[4] H. Matsuno, A. Yokoyama, F. Watari, M. Uo, T. Kawasaki, Biomater. 22 (2001) 1253-1262.

[5] J. Black, Clinical Mater. 16 (1994) 167-173.

[6] J.B. Clark, R.K. Garrett Jr., T.L. Jungling, R.I. Asfahani, Metall. Trans. A. 22 (1991) 2959-2968.

[7] C.L. Briant, E. MacDonald, R.W. Balliet, T. Luong, Int. J. Refract. Met. Hard Mater. 18 (2000) 1-8.

[8] E.O. Hall, (1951) Proc. Phys. Soc. B 64 (1951) 747-753.

[9] N.J. Petch, J. Iron Steel Inst. 174 (1953) 25-28.

[10] R.Z. Valiev, R.K. Islamgaliev, I.V. Alexadrov, Prog. Mater. Sci. 45 (2000) 103-189.

[11] T.G. Langdon, Acta Mater. 61 (2013) 7035-7059.

[12] Y. Huang, T.G. Langdon, Mater. Today 16 (2013) 85-92.

[13] R.Z. Valiev, T.G. Langdon, Prog. Mater. Sci. 51(2006) 881-981.

[14] A.P. Zhilyaev, T.G. Langdon, Prog. Mater. Sci. 53 (2008) 893-979.

[15] A.P. Zhilyaev, B.-K. Kim, G.V. Nurislamova, M.D. Baró, J.A. Szpunar, T.G. Langdon, Scripta Mater. 46 (2002) 575-580.

[16] A.P. Zhilyaev, G.V. Nurislamova, B.-K. Kim, M.D. Baró, J.A. Szpunar, T.G. Langdon, Acta Mater. 51 (2003) 753-765.

[17] J. Wongsa-Ngam, M. Kawasaki, T.G. Langdon, J. Mater. Sci. 48 (2013) 4653-4660.

[18] S.N. Mathaudhu, K.T. Hartwig, Mater. Sci. Eng. A 426 (2006) 128-142.

[19] S.N. Mathaudhu, K.T. Hartwig, Mater. Sci. Eng. A 463 (2007) 94-100.

[20] Q. Wei, B.E. Schuster, S.N. Mathaudhu, K.T. Hartwig, L.J. Kecskes, R.J. Dowding, K.T. Ramesh, Mater. Sci. Eng. A 493 (2008) 58-64.

[21] E. Hosseini, M. Kazeminezhad, Intl. J. Refract. Metals Hard Mater. 27 (2009) 605-619.

[22] Q. Wei, Z.L. Pan, X.L. Wu, B.E. Schuster, L.J. Kecskes, R.Z. Valiev, Acta Mater. 59 (2011) 2423-2436.

[23] K. Edalati, Z. Horita, Acta Mater. 59 (2011) 6831-6836.

[24] K. Edalati, Z. Horita, Scripta Mater. 64 (2011) 161-164.

[25] J.P. Ligda, B.E. Schuster, Q. Wie, Scripta Mater. 67 (2012) 253-256.

[26] C.H. Lu, B.A. Remington, B.R. Maddox, B. Kad, H.S. Park, M. Kawasaki, T.G. Langdon, M.A. Meyers, Acta Mater. 61 (2013) 7767-7780.

[27] Y. Huang, N. Maury, N.X. Zhang, T.G. Langdon, IOP Conf. Series: Mater. Sci. Eng. 63 (2014) 012100.

[28] R.B. Figueiredo, P.R. Cetlin, T.G. Langdon, Mater. Sci. Eng. A 528 (2011) 8198-8204.

[29] R.B. Figueiredo, P.H.R. Pereira, M.T.P. Aguilar, P.R. Cetlin, T.G. Langdon, Acta Mater. 60 (2012) 3190-3198.

[30] M. Kawasaki, T.G. Langdon, Mater. Sci. Eng. A 498 (2008) 341-348.

[31] H.M. Rietveld, J. Appl. Crystall. 2 (1969) 65-71.

[32] A. Loucif, R.B. Figueiredo, M. Kawasaki, T. Baudin, F. Brisset, R. Chemam, T.G. Langdon, J. Mater. Sci. 47 (2012) 7815-7820.

[33] L.S. Tóth, B. Beausir, C.F. Gu, Y. Estrin, N. Scheerbaum, C.H.J. Davies, Acta Mater. 58 (2010) 6706-6716.

[34] Y.H. Zhao, K. Zhang, K. Lu, Phys. Rev. B 56 (1997) 14322.

[35] Y.H. Zhao, H.W. Sheng, K. Lu, Acta Mater. 49 (2001) 365-375.

[36] Y.H. Zhao, Y.T. Zhu, X.Z. Liao, Z. Horita, T.G. Langdon, Mater. Sci. Eng. A 463 (2007) 22-26.

[37] K. Máthis, J. Gubicza, N.H. Nam, J. Alloys Compd. 394 (2005) 194-199.

[38] I. Semenova, G. Salimgareeva, G. Da Costa, W. Lefebvre, R. Valiev, Adv. Eng. Mater. 12 (2010) 803-807.

[39] A.V. Polyakov, I.P. Semenova, R.Z. Valiev, Y. Huang, T.G. Langdon, MRS Commun. 3 (2013) 249-253.

[40] A.V. Polyakov, I.P. Semenova, Y. Huang, R.Z. Valiev, T.G. Langdon, Adv. Eng. Mater. 16 (2014) 1038-1043.

[41] O. Andreau, J. Gubicza, N.X. Zhang, Y. Huang, P. Jenei, T.G. Langdon, Mater. Sci. Eng. A 615 (2014) 231-239.

[42] R.Z. Valiev, YuV. Ivanisenko, E.F. Rauch, B. Baudelet, Acta Mater. 44 (1996) 4705-4712.

[43] F. Wetscher, A. Vorhauer, R. Stock, R. Pippan, Mater. Sci. Eng. A 387–389 (2004) 809-816.

[44] F. Wetscher, R. Pippan, S. Sturm, F. Kauffmann, C. Scheu, G. Dehm, Metall. Mater. Trans. A 37 (2006) 1963-1968.

[45] Y. Estrin, A. Molotnikov, C.H.J. Davies, R. Lapovok, J. Mech. Phys. Solids 56 (2008) 1186-1202.

[46] E.N. Popova, V.V. Popov, E.P. Romanov, V.P. Pilyugin, Phys. Metals Metall. 103 (2007) 407-413.

[47] V.V. Popov, E.N. Popova, A.V. Stolbovskii, V.P. Pilyugin, N.K. Arkhipova, Phys. Metals Metall. 113 (2012) 295-301.

[48] C.F. Gu, L.S. Tóth, S. Rusz, M. Bova, Scripta Mater. 86 (2014) 36-39.

[49] M. Ahlers, Metall. Trans. 1 (1970) 2415-2428.

[50] G.K. Williamson, R.E. Smallman, Philos. Mag. 1 (1956) 34-46.

[51] R.E. Smallman, K.H. Westmacott, Philos. Mag. 2 (1957) 669-683.

[52] Y.H. Zhao, X.Z. Liao, Z. Jin, R.Z. Valiev, Y.T. Zhu, Mater. 52 (2004) 4589-4599.

[53] A. Vorhauer, R. Pippan, Scripta Mater. 51 (2004) 921-925.

[54] M. Kawasaki, B. Ahn, T.G. Langdon, Acta Mater. 58 (2010) 919-930.

[55] M. Kawasaki, B. Ahn, T.G. Langdon, Mater. Sci. Eng. A 527 (2010) 7008-7016.

[56] M. Kawasaki, J. Mater. Sci. 49 (2014) 18-34.

[57] R.Z. Valiev, I.V. Alexandrov, Y.T. Zhu, T.C. Lowe, J. Mater. Res. 17 (2002) 5-8.

[58] T. Mungole, P. Kumar, M. Kawasaki, T.G. Langdon, J. Mater. Res. 29 (2014) 2534-2546.

[59] T. Mungole, P. Kumar, M. Kawasaki, T.G. Langdon, J. Mater. Sci. 50 (2015) 3549-3561.

Figure captions

Fig. 1 Representative microstructures after HPT processing: (a) and (b) show the edge and centre areas after 0.5 turn, (c) and (d) show the edge areas after 1 and 5 turns and (e) and (f) show the edge and centre areas after 10 turns.

Fig. 2 Grain size distributions after HPT processing: (a), (b), (c) and (d) show the edge areas after 0.5, 1, 5 and 10 turns and (e) shows the centre area after 10 turns.

Fig. 3 Distributions of grain boundary misorientations: (a) and (b) show the edge and centre areas after 0.5 turn, (c) and (d) show the edge areas after 1 and 5 turns, and (e) and (f) show the edge and centre areas after 10 turns.

Fig. 4 Colour-coded maps showing the distributions of the Vickers microhardness values over discs processed by HPT through 0.5, 1, 2, 5 and 10 turns: the colour key is shown on the lower right.

Fig. 5 X-ray diffraction patterns for the as-received material and after processing by HPT through 1, 5 and 10 turns.

Fig. 6 Crystallite size and microstrain estimated from an analysis of the XRD peak broadening and shown as a function of the number of turns.

Fig. 7 Stress-strain curves at a strain rate of 1.0×10^{-3} s^{-1} for the as-received material and after HPT processing and HPT plus short-term annealing at 873 and 973 K: for (a) 1 turn, (b) 5 turns and (c) 10 turns.

Fig. 8 The estimated dislocation density shown as a function of the numbers of turns.

Fig. 9 Values of the Vickers microhardness plotted as a function of the equivalent strain in discs processed by HPT for 0.5, 1, 2, 5 and 10 turns.

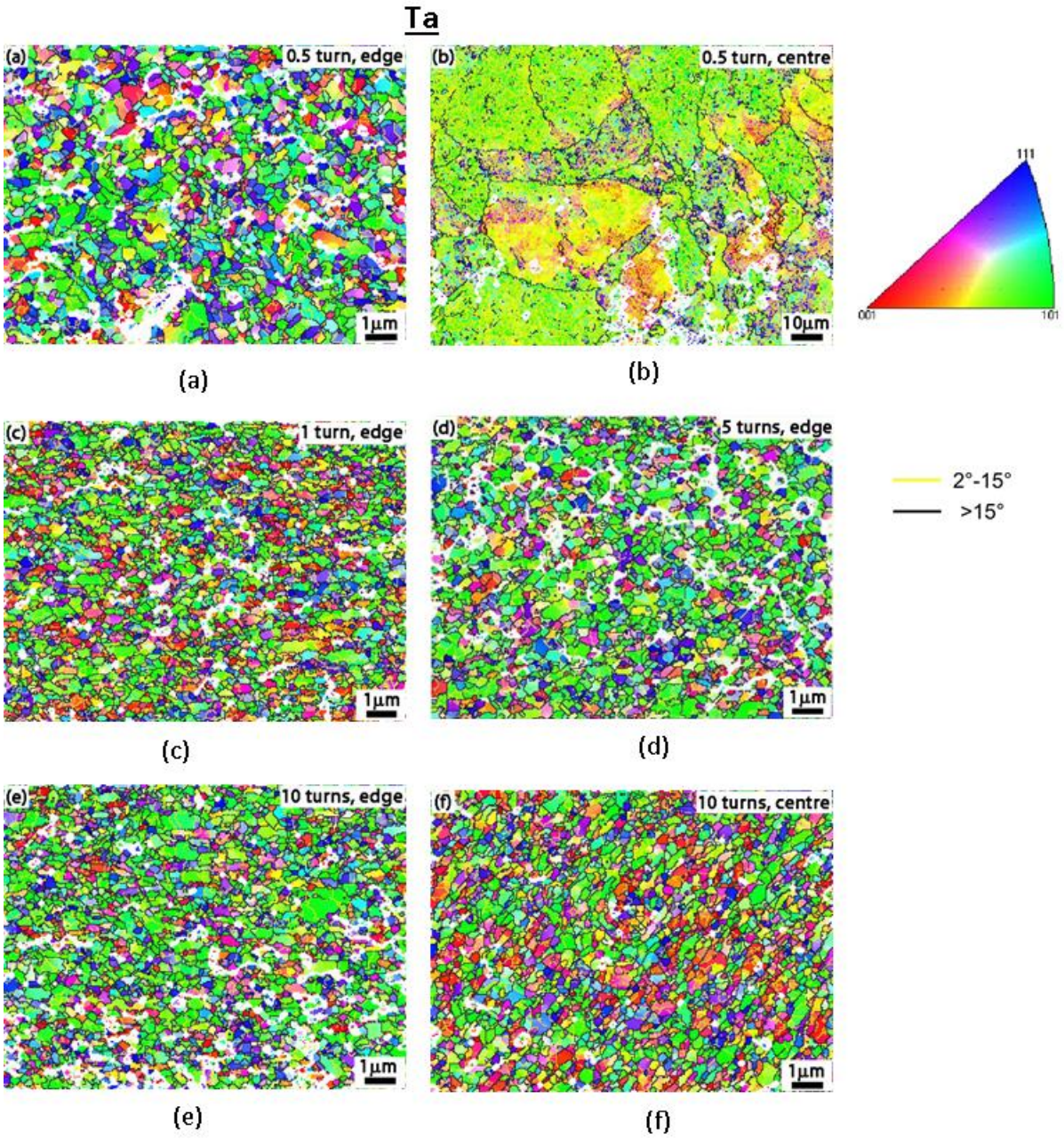
Ta
(a)
0.5 turn, edge
1μm
(b)
0.5 turn, centre
10μm
111
001
101
(a)
(b)
(c)
1 turn, edge
1μm
(d)
5 turns, edge
1μm
2°-15°
>15°
(c)
(d)
(e)
10 turns, edge
1μm
(f)
10 turns, centre
1μm
(e)
(f)

Fig. 1

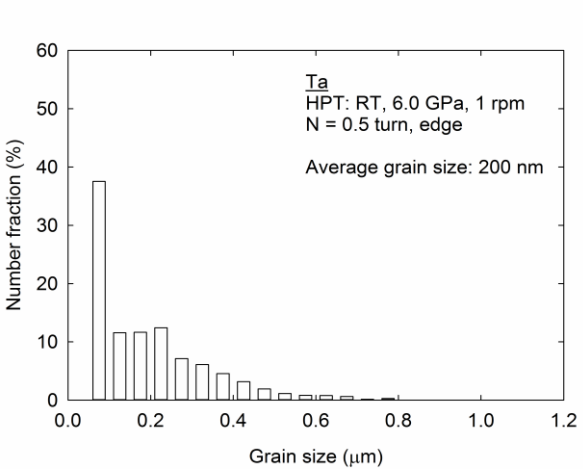
Ta
HPT: RT, 6.0 GPa, 1 rpm
N = 0.5 turn, edge
Average grain size: 200 nm
Number fraction (%)
Grain size (μm)

(a)

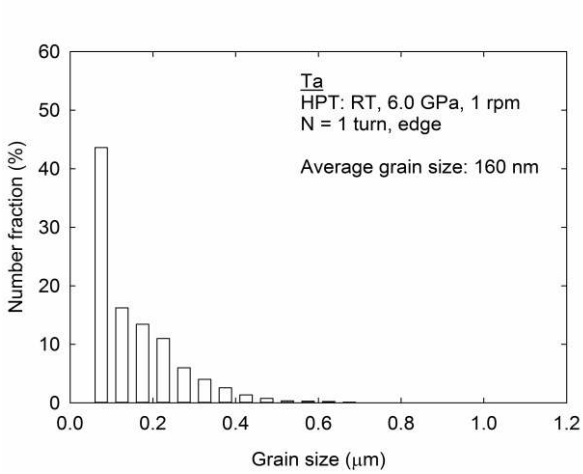
Ta
HPT: RT, 6.0 GPa, 1 rpm
N = 1 turn, edge
Average grain size: 160 nm
Number fraction (%)
Grain size (μm)

(b)

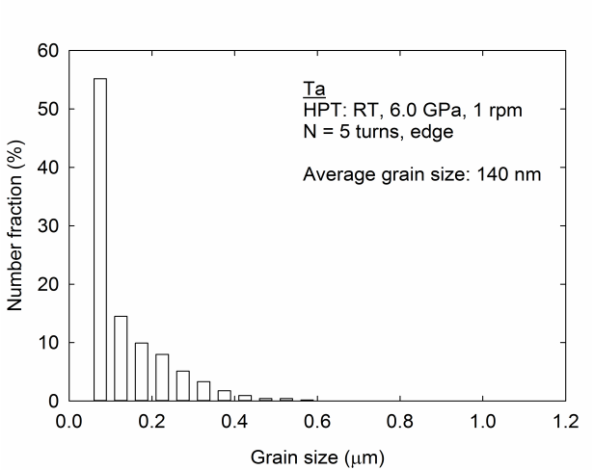
Ta
HPT: RT, 6.0 GPa, 1 rpm
N = 5 turns, edge
Average grain size: 140 nm
Number fraction (%)
Grain size (μm)

(c)

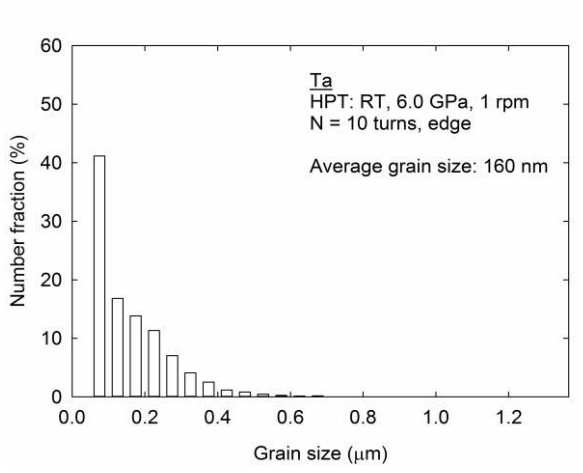
Ta
HPT: RT, 6.0 GPa, 1 rpm
N = 10 turns, edge
Average grain size: 160 nm
Number fraction (%)
Grain size (μm)

(d)

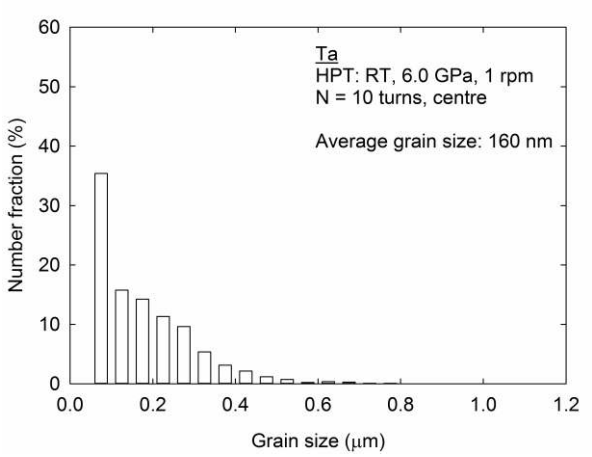
Ta
HPT: RT, 6.0 GPa, 1 rpm
N = 10 turns, centre
Average grain size: 160 nm
Number fraction (%)
Grain size (μm)

(e)

Fig. 2

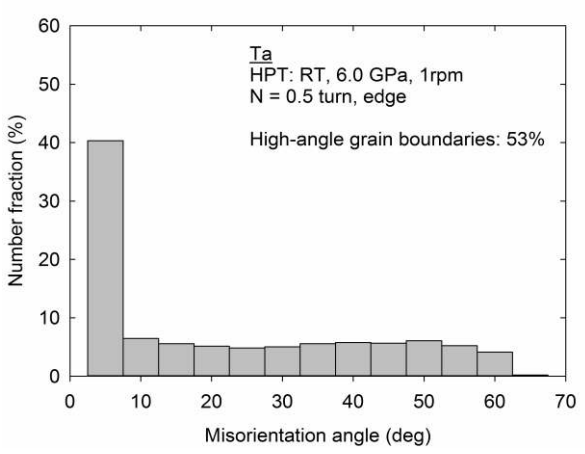
Ta
HPT: RT, 6.0 GPa, 1rpm
N = 0.5 turn, edge
High-angle grain boundaries: 53%
Number fraction (%)
Misorientation angle (deg)

(a)

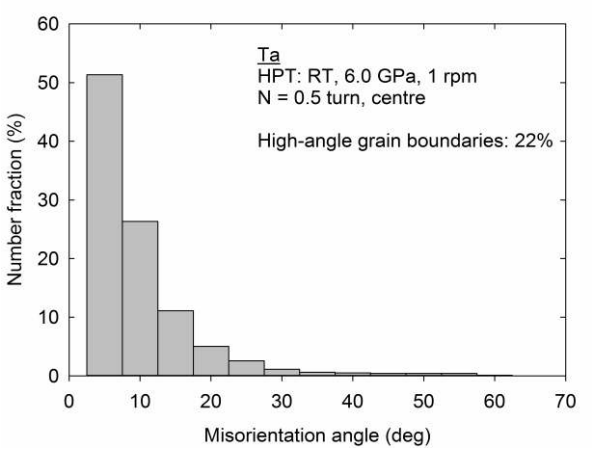
Ta
HPT: RT, 6.0 GPa, 1 rpm
N = 0.5 turn, centre
High-angle grain boundaries: 22%
Number fraction (%)
Misorientation angle (deg)

(b)

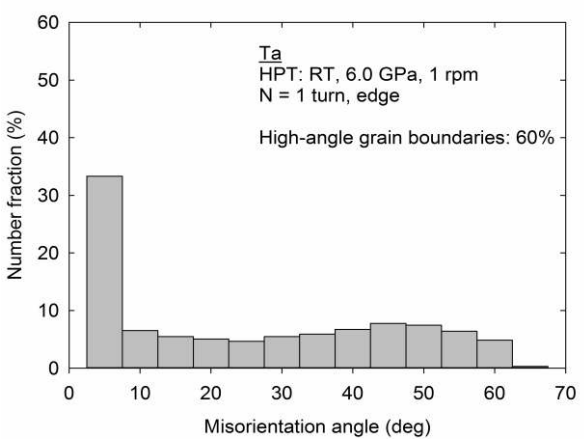
Ta
HPT: RT, 6.0 GPa, 1 rpm
N = 1 turn, edge
High-angle grain boundaries: 60%
Number fraction (%)
Misorientation angle (deg)

(c)

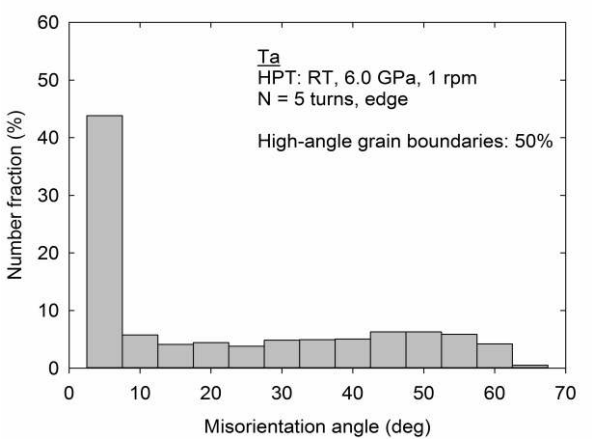
Ta
HPT: RT, 6.0 GPa, 1 rpm
N = 5 turns, edge
High-angle grain boundaries: 50%
Number fraction (%)
Misorientation angle (deg)

(d)

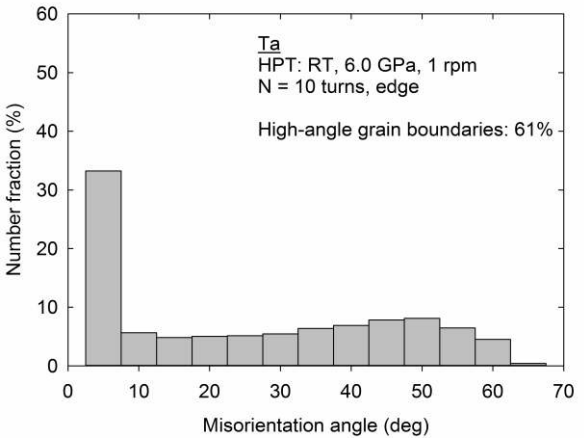
Ta
HPT: RT, 6.0 GPa, 1 rpm
N = 10 turns, edge
High-angle grain boundaries: 61%
Number fraction (%)
Misorientation angle (deg)

(e)

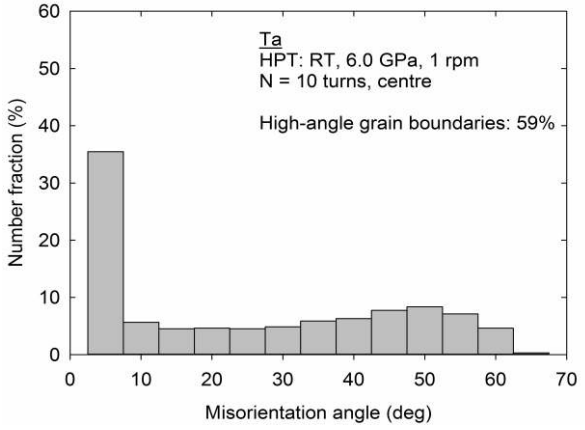
Ta
HPT: RT, 6.0 GPa, 1 rpm
N = 10 turns, centre
High-angle grain boundaries: 59%
Number fraction (%)
Misorientation angle (deg)

(f)

Fig. 3

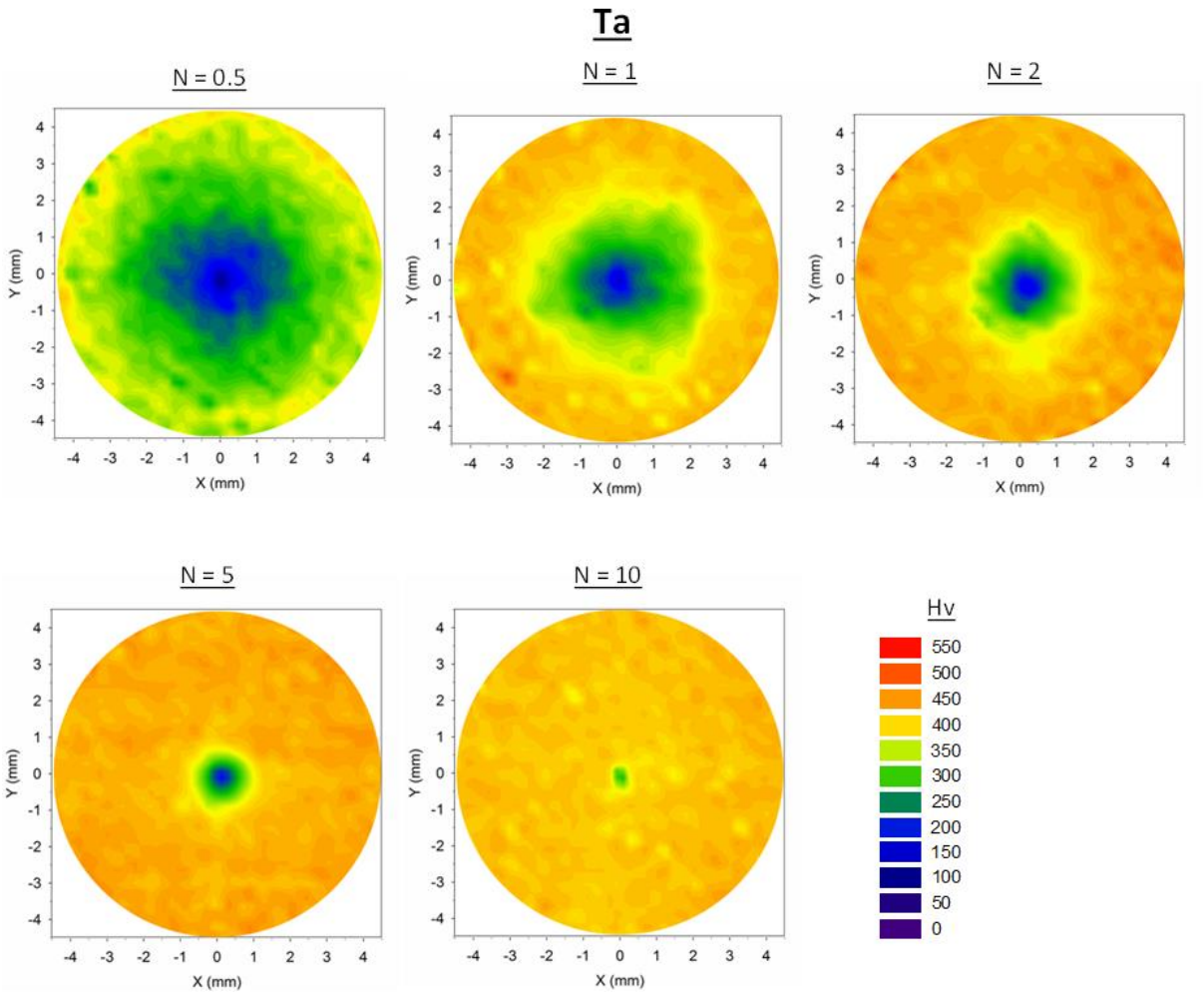
Ta
N = 0.5
N = 1
N = 2
N = 5
N = 10
Y (mm)
X (mm)
Hv
550
500
450
400
350
300
250
200
150
100
50
0

Fig. 4

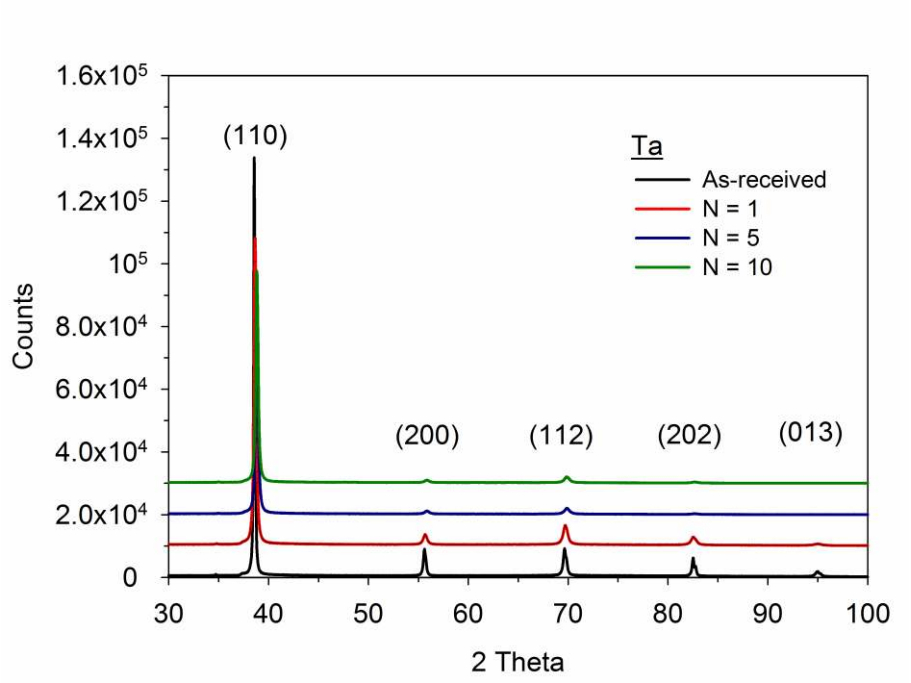
1.6x10^5
1.4x10^5
1.2x10^5
10^5
8.0x10^4
6.0x10^4
4.0x10^4
2.0x10^4
0
Counts
(110)
(200)
(112)
(202)
(013)
Ta
As-received
N = 1
N = 5
N = 10
30
40
50
60
70
80
90
100
2 Theta

Fig. 5

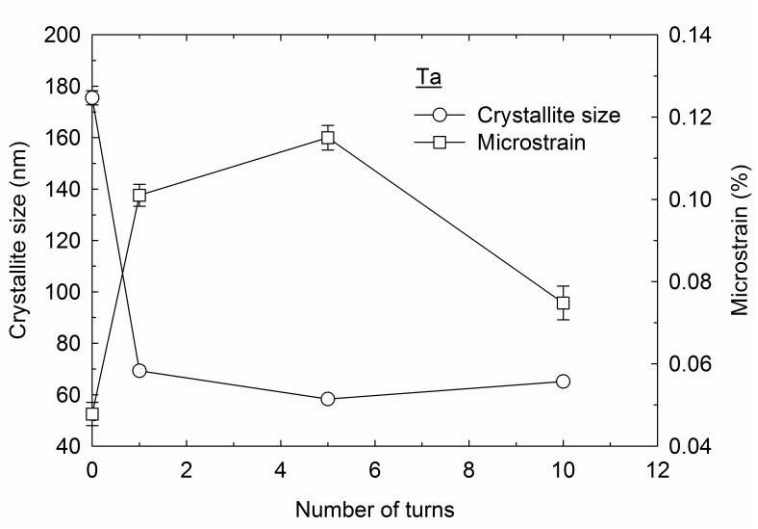
Ta
Crystallite size
Microstrain
Crystallite size (nm)
Microstrain (%)
Number of turns
200
180
160
140
120
100
80
60
40
0.14
0.12
0.10
0.08
0.06
0.04
0
2
4
6
8
10
12

Fig. 6

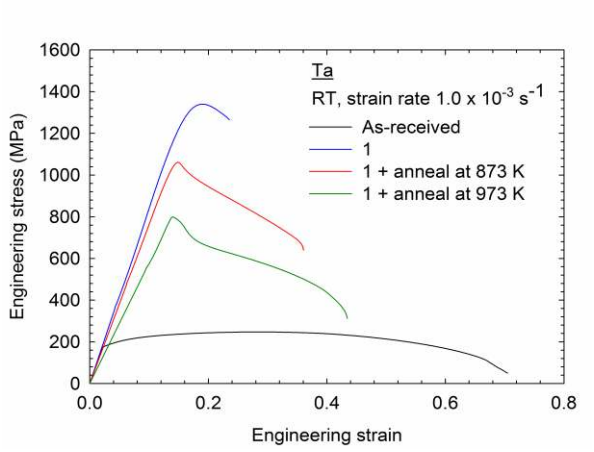
Ta
RT, strain rate 1.0 x 10-3 s-1
As-received
1
1 + anneal at 873 K
1 + anneal at 973 K
Engineering stress (MPa)
Engineering strain
0
200
400
600
800
1000
1200
1400
1600
0.0
0.2
0.4
0.6
0.8

(a)

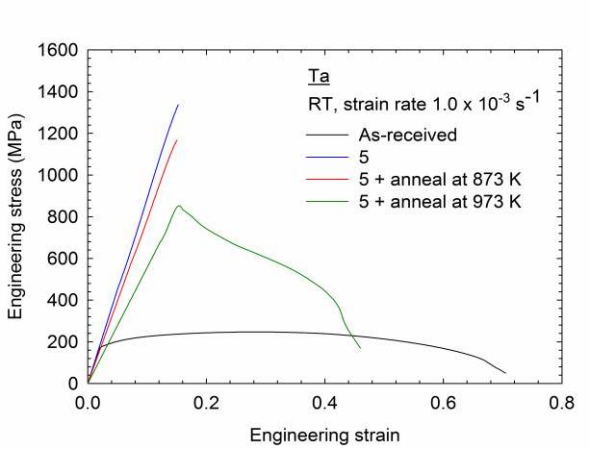
Ta
RT, strain rate 1.0 x 10-3 s-1
As-received
5
5 + anneal at 873 K
5 + anneal at 973 K
Engineering stress (MPa)
Engineering strain
0
200
400
600
800
1000
1200
1400
1600
0.0
0.2
0.4
0.6
0.8

(b)

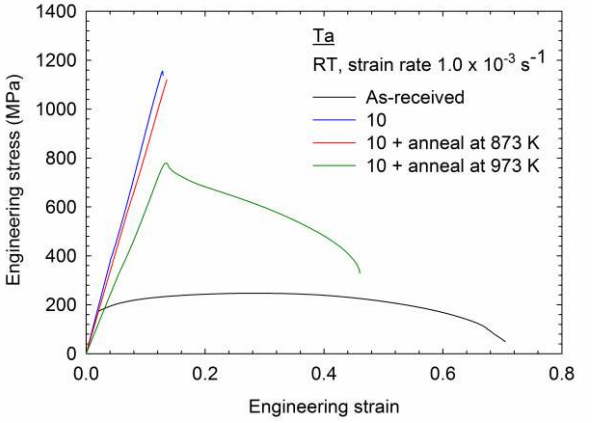
Ta
RT, strain rate 1.0 x 10-3 s-1
As-received
10
10 + anneal at 873 K
10 + anneal at 973 K
Engineering stress (MPa)
Engineering strain
0
200
400
600
800
1000
1200
1400
0.0
0.2
0.4
0.6
0.8

(c)

Fig. 7

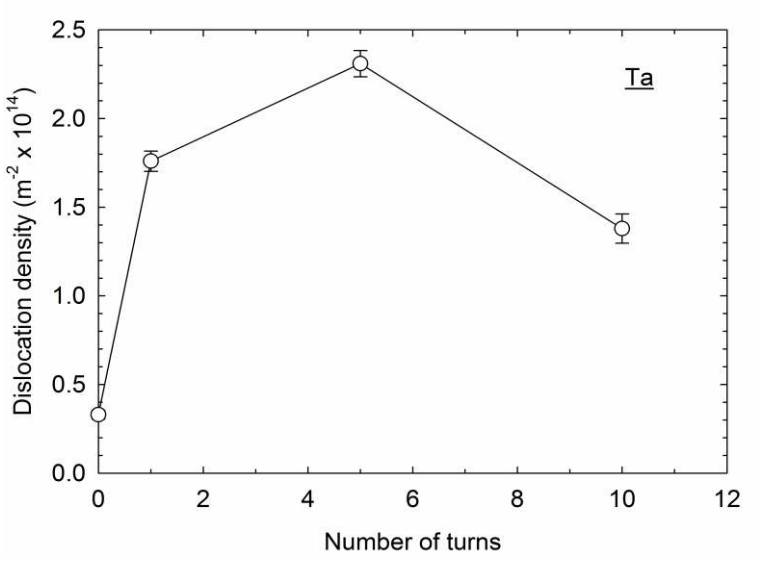
Ta
Dislocation density (m^{-2} x 10^{14})
Number of turns
0.0
0.5
1.0
1.5
2.0
2.5
0
2
4
6
8
10
12

Fig. 8

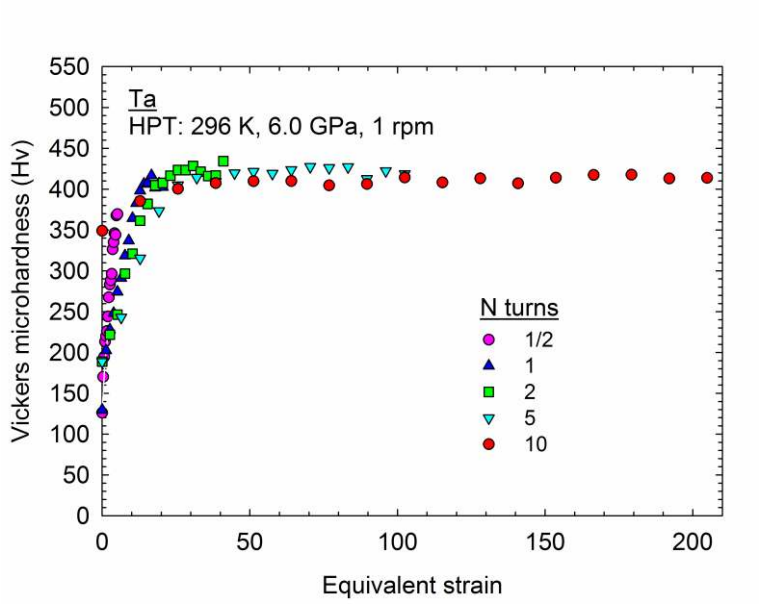
Ta
HPT: 296 K, 6.0 GPa, 1 rpm
Vickers microhardness (Hv)
Equivalent strain
N turns
1/2
1
2
5
10
0
50
100
150
200
0
50
100
150
200
250
300
350
400
450
500
550

Fig. 9